PCCP

ROYAL SOCIETY OF CHEMISTRY

PAPER

View Article Online
View Journal | View Issue

Cite this: *Phys. Chem. Chem. Phys.*, 2020, **22**, 3105

A study on the effects of mixed organic cations on the structure and properties in lead halide perovskites†

Chao Wu, [a] Daoyou Guo, [a] Peigang Li,*[b] Shunli Wang,*[a] Aiping Liu[a] and Fengmin Wu*[a]

Received 15th November 2019,
Accepted 7th January 2020

DOI: 10.1039/c9cp06182g

rsc.li/pccp

Recently, organic-lead halide perovskites have emerged as strong competitors in photovoltaic and general optoelectronic applications owing to their remarkable characteristics, including high balance hole and electron mobility, strong absorption coefficient and long carrier lifetime. However, the commercial applicability of these materials is hampered by their relative lack of stability compared to established inorganic and organic semiconductors. It has been found that it is possible to tune the properties and stability of the organic-lead halide perovskite materials by site-substitution at A sites of the ABX_3 perovskite structure. Here, organic cations (NH_4^+, HC $(NH_2)_2^+$, and $CH_3CH_2NH_3^+$) were successfully incorporated in the methylammonium-based perovskite crystal to investigate the role of organic cation size on structure, optical features, thermal stability, and electrical transport properties. Powder X-ray diffraction results indicate that the size of organic cations can not only cause lattice strain by lattice contraction or dilation but also may induce phase transitions by octahedral tilting. Meanwhile, band gaps of these crystals show that organic cations could tune the band gap energy of the perovskites by changing the Pb–I bond angle, which agrees with previous reports. The result of thermogravimetric analysis indicates that thermal stability is related to the probability of HI formation, which is directly related to the acidity of the organic species. These results represent an important step to highlight the role of organic cations in hybrid perovskite materials, which will further benefit the fundamental understanding of materials and device optimization.

Introduction

Recently, organic-lead halide perovskites have been widely investigated on account of their remarkable characteristics, including direct band gap, high balance hole and electron mobility, strong absorption coefficient, and long carrier lifetimes.[1–3] Due to their superior characteristics the organic-lead halide perovskites have emerged as strong competitors in photovoltaic and general optoelectronic applications. The organic-lead halide perovskite-based solar cells have more than 23.6% power conversion efficiency (PCE), making them favorable for commercialization.[4] However, the commercial applicability of these materials is hampered by their relative lack of stability compared to established inorganic and organic semiconductors. It has been found that it is possible to tune the properties and stability of the organic-lead halide perovskite materials by site-substitution at A sites of the ABX_3 perovskite structure.[5]

Currently, research on methylammonium (MA) lead iodide ($MAPbI_3$) and formamidinium (FA) lead iodide ($FAPbI_3$) has become a hot topic worldwide and the number of publications shows the exponential growth as a function of time on the logarithmic scale. $MAPbI_3$ crystals have a tetragonal structure at room temperature, which suffers from lattice distortion and strain, while $FAPbI_3$ crystals suffer from the well-known spontaneous phase transition from the desired cubic phase (α phase) black perovskite to δ-phase yellow non-perovskite at room temperature. This phase transition is the main obstacle for high efficiency and long-term stability of $MAPbI_3$-based and $FAPbI_3$-based optoelectronic devices. Meanwhile, the optical response range and decomposition temperature of these organic-lead halide perovskites are unsatisfactory for optoelectronic applications.

Composition engineering could be a potential solution to solve these problems. Seok *et al.*[6] prepared $MA_xFA_{1-x}PbI_3$

[a] *Department of Physics, Center for Optoelectronics Materials and Devices, Zhejiang Sci-Tech University, Hangzhou, 310018, China. E-mail: slwang@zstu.edu.cn, wfm@zstu.edu.cn*
[b] *State Key Laboratory of Information Photonics and Optical Communications & Laboratory of Information Functional Materials and Devices, School of Science, Beijing University of Posts and Telecommunications Beijing, 100876, China. E-mail: pgli@zstu.edu.cn*

† Electronic supplementary information (ESI) available. See DOI: 10.1039/c9cp06182g

perovskite thin films by mixing the large FA cation with the small MA cation, resulting in a tunable band gap and a stable structure. Zhu *et al.*[7] had synthesized the mixed $FA_{1-x}Cs_xPbI_3$ perovskite thin films with a Cs component between 0.1 and 0.3, which provided an expected improvement in thermal stability. However, most published reports are based on polycrystalline films, which invariably contain significant grain boundaries and defects due to their preparation processes. These defects limit their applications in high performance devices. More importantly, it is still not clear what role organic cations play, nor how they influence the material properties in perovskites.

To obtain a deeper understanding of material properties, single crystals are regarded as the best platform among various building blocks for fundamental study. Here, we synthesized a series of perovskite single crystals with mixed organic cations (NH_4^+, MA^+, $HC(NH_2)_2^+$=FA, $CH_3CH_2NH_3^+$=EA) along the compositional space, and conducted a systematic investigation to correlate the carrier behavior with the organic cation size. The single crystals were synthesized *via* inverse temperature crystallization assisted by hydroiodic acid, where the quality of the crystals could be judiciously controlled by the thermodynamic process. It is found that size of the organic cation can not only cause lattice strain by lattice contraction or dilation but also may induce phase transitions by octahedral tilting. Meanwhile, thermal stability is related to the probability of HI formation, which is directly related to the acidity of the organic species. FA incorporated $MAPbI_3$ crystals possess the best thermodynamic properties owing to the low acidity of the FA cation. Organic cations affect transport properties of crystals by affecting crystal structure. The cubic phase crystals have the lowest lattice strain and low trap density. These results represent an important step to highlight the role of organic cations in hybrid perovskite materials, which will further benefit the fundamental understanding of materials and device optimization.

Experimental

Synthesis of mixed-perovskite crystals

Growth of the mixed-perovskite crystals. Perovskite crystals were grown using a reported method of inverse temperature crystallization.[8] Briefly, 1 M PbI_2 and 1 M MAI were dissolved in 2 ml γ-butyrolactone (GBL) at 40 °C, and stirred until the solution become clear. The solution was then kept at 90 °C for about 12 h to allow for pure $MAPbI_3$ crystal growth. For the FA cation mixed with $MAPbI_3$, 0.159 g MAI, and 0.172 g FAI were dissolved in 2 ml GBL solution, for the EA cation mixed with $MAPbI_3$, 0.273 g MAI, and 0.05 g EAI were dissolved in 2 ml GBL solution and for the NH_4 cation mixed with $MAPbI_3$, 0.238 g MAI, and 0.01 g NH_4I were dissolved in 2 ml GBL solution.

Characterization of the mixed-perovskite crystals

Powder X-ray diffraction (XRD) data of the single crystals were collected by X-ray diffraction (Bruker D8-Advance) using Cu Kα radiation. UV-vis diffuse reflectance spectrums were measured by UV-vis diffuse reflectance spectroscopy (U-3900). Thermogravimetric analysis (TGA) was performed on a TGA analyzer (PYRTS 1). Differential scanning calorimetry (DSC) analysis was carried out by using a Q2000 to test phase transition. UV-vis diffuse reflectance spectroscopy was carried out using a UV-vis spectrophotometer (U-3900). *V–I* characteristics were tested using a Keithley 2400 instrument.

Result and discussion

Four types of organic cation-mixed single crystals were successfully grown by the inverse temperature crystallization process. All crystals are of millimeter size, as shown in Fig. 1. In principle, any single-charged organic cation could be used to form a perovskite once there is sufficient space to fit it within the inorganic crystalline cage. But, if a cation is oversized, a perovskite with a low dimension crystal structure will form. In our work, all crystals form 3D structures. In this structure, the halogen, I, atoms occupy the vertices of corner-sharing BX_6 octahedra, while the divalent metal, Pb, sits at the center of the octahedron. Organic species occupy the 12-coordinated octahedral cavities of the 3D network. A schematic diagram of crystal structure is shown in Fig. 2(d).

To further investigate the crystal structure, single crystals were ground into powder to characterize their crystalline phase by powder X-ray diffraction. As shown in Fig. 2(a) and (b), all samples possess a pure perovskite phase. The main peaks for $MAPbI_3$ and NH_4^+-incorporated $MAPbI_3$(NH_4@$MAPbI_3$) crystals are at about $2\theta = 14.1^\circ$, 28.3°, and 31.7°, which is in agreement with that of a previously reported pure tetragonal phase.[9] The reported, calculated and experimental data of $MAPbI_3$ show that (211) and (213) intensity peaks were used to differentiate between tetragonal and cubic phases.[10] No (211) reflection at $2\theta = 23.5^\circ$ was observed, which proves that EA^+-incorporated $MAPbI_3$ crystal (EA@$MAPbI_3$) and FA^+-incorporated $MAPbI_3$

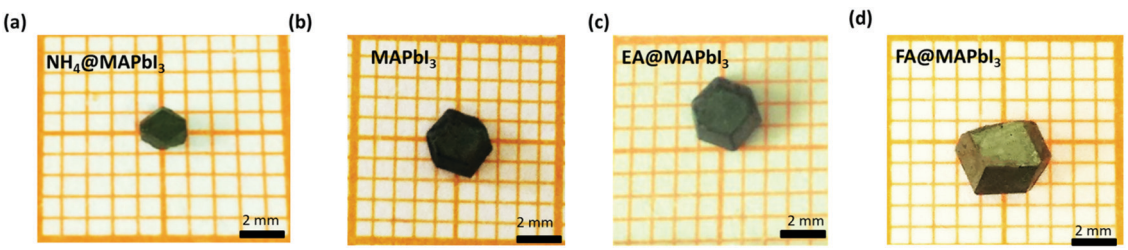

Fig. 1 Images of single crystals (a) NH_4@$MAPbI_3$; (b) $MAPbI_3$; (c) EA@$MAPbI_3$; (d) FA@$MAPbI_3$.

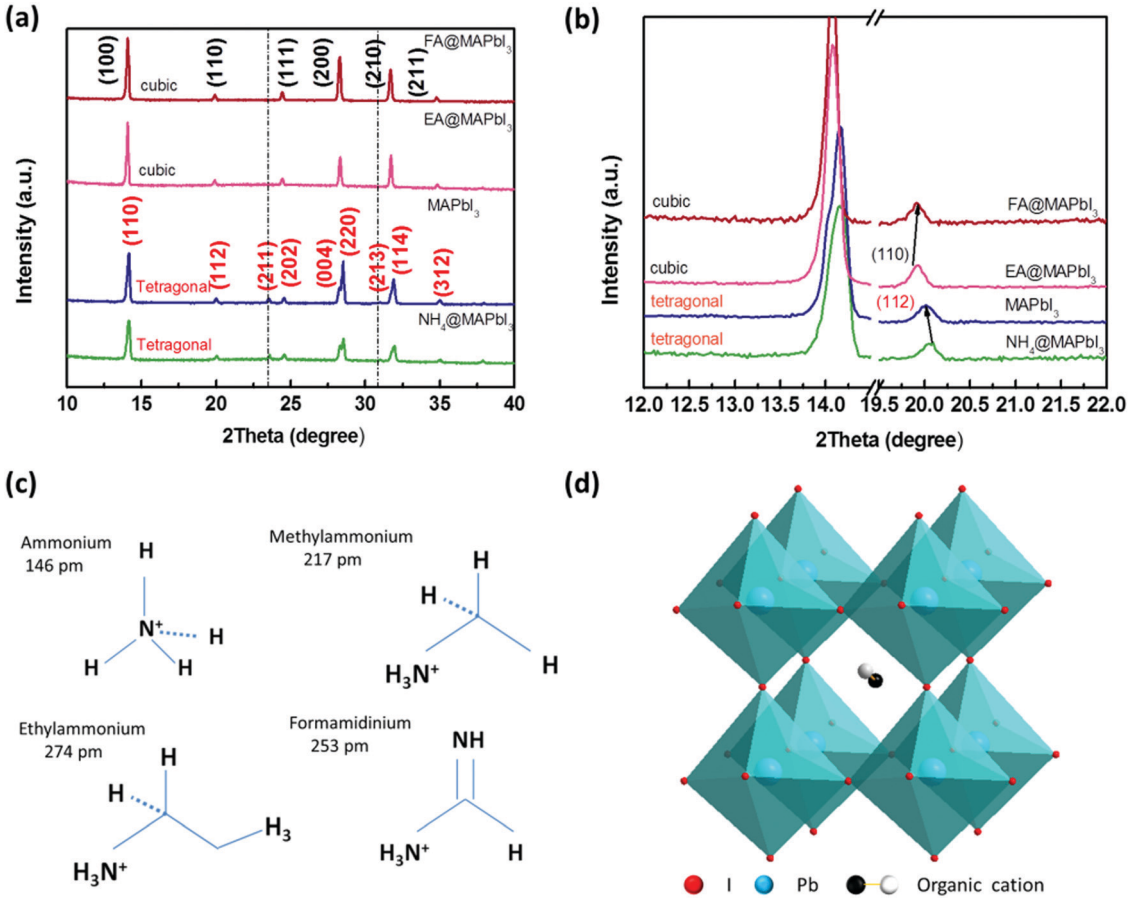

Fig. 2 (a and b) Powder XRD patterns of the perovskite crystals. (c) Sizes of the organic cations. (d) Crystal structure of the A-site organic cation mixed perovskite.

Table 1 Cell parameters of NH_4@$MAPbI_3$, $MAPbI_3$, EA@$MAPbI_3$ and FA@$MAPbI_3$crystals

Parameter	NH4@$MAPbI_3$	$MAPbI_3$	EA@$MAPbI_3$	FA@$MAPbI_3$
Symmetry	Tetragonal	Tetragonal	Cubic	Cubic
Space group	*I*4/*mcm*	*I*4/*mcm*	*Pm*$\bar{3}$*m*	*Pm*$\bar{3}$*m*
a (Å)	8.879	8.931	6.308	6.328
b (Å)	8.879	8.931	6.308	6.328
c (Å)	12.664	13.032	6.308	6.328

crystal (FA@$MAPbI_3$) have a cubic structure. Cell parameters of the four types of crystals are shown in Table 1. The expanded powder XRD patterns of the four types of crystals are shown in Fig. S1, ESI.† The (112) peak diffraction in Fig. 2(b) shifts to a higher angle when the small sized cation NH_4^+ is incorporated into a MA-based perovskite. Simultaneously, when the A-site cation is changed from EA@MA to FA@MA, the (110) peak diffraction shifted to a lower angle. These peak diffraction shifts are the result of a variation of lattice parameters in the crystals upon the partial substitution of the organic cation. The sizes of the organic cations are shown in Fig. 2(c). The powder X-ray diffraction data show that when an EA cation or FA cation is incorporated, the $MAPbI_3$ structure transited from a tetragonal phase to a cubic phase. Octahedral tilting has been proven to be the origin of phase transition in perovskite crystals.[11] This octahedral tilt adjusts the tolerance factor toward the first distortion factor, which results in favorable conditions to stabilize cubic perovskites.[12] In contrast, if a small cation such as NH_4^+ is incorporated into $MAPbI_3$, the lattice of the cell contracts and the tolerance factor shifts far away from the distortion factor 1; hence NH4@$MAPbI_3$ still retains a tetragonal structure. In summary, the size of the cation could tune the structure of lead halide perovskites *via* lattice contracting and octahedral tilting.

UV-vis diffuse reflectance spectra of perovskites were characterized by a UV-vis diffuse reflectance spectrometer to confirm the band gap energy of single crystals. Diffuse reflectance spectra for the single crystals as a function of wavelength in the range of 740–860 nm are presented in Fig. 3(a). The absorption edges of $MAPbI_3$ and EA@$MAPbI_3$ are about 830 nm, while the absorption edge of NH_4@$MAPbI_3$ maintains a blue-shift to about 820 nm. The absorption edge of the FA@$MAPbI_3$ crystal displays a clear red-shift to ~860 nm. The red-shift of the absorption edge allows the perovskite to function as an efficient solar cell light-absorbing material. A further analysis of optical spectra can be performed to calculate band gap energy. The Kubelka–Munk equation at any wavelength is:

$$\frac{K}{S} = \frac{(1 - R_\infty)}{2R_\infty} = F(R_\infty) \quad (1)$$

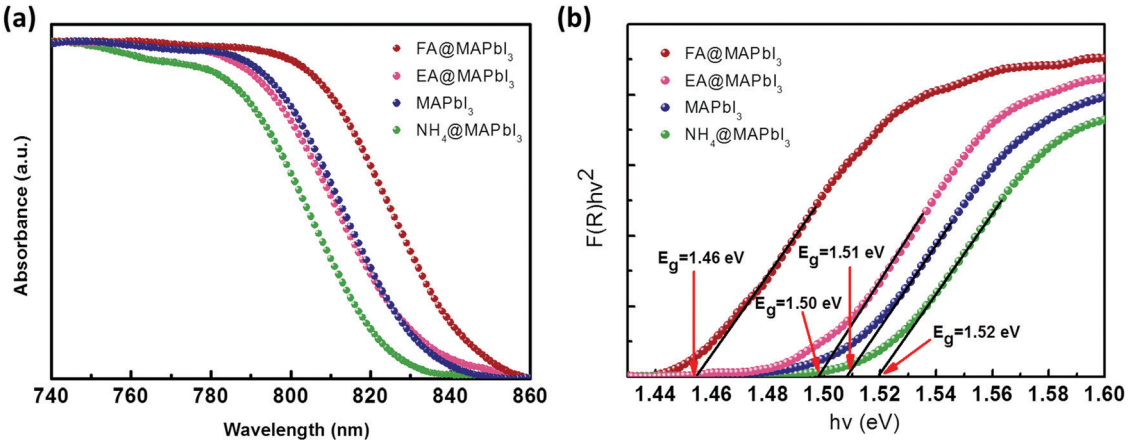

Fig. 3 (a) UV-vis diffuse reflectance spectra for mixed-perovskite crystals. (b) Band gap energy determination.

where S and K are scattering and absorption coefficients, respectively, and $F(R_\infty)$ is the Kubelka–Munk function. The band gap E_g and the absorption coefficient α of a direct band gap semiconductor are related through the well-known equation:[13,14]

$$\alpha h\nu = C_1\left(h\nu - E_g\right)^{\frac{1}{2}} \quad (2)$$

where α is the linear absorption coefficient of the material, $h\nu$ is the photon energy, and C_1 is a proportionality constant. When the material scatters in a perfectly diffuse manner, the Kubelka–Munk absorption coefficient S is constant with respect to wavelength, and using the remission function in eqn (2), we obtain the expression:[15]

$$[F(R_\infty)h\nu]^2 = C_2(h\nu - E_g) \quad (3)$$

Therefore, obtaining $F(R_\infty)$ from eqn (1) and plotting $[F(R_\infty)h\nu]^2$ against $h\nu$, the band gap energies, E_g, can be obtained easily, and are shown in Fig. 3(b). The band gap energies of NH_4@$MAPbI_3$, $MAPbI_3$, EA@$MAPbI_3$, and FA@$MAPbI_3$ are 1.52, 1.51, 1.50, and 1.46 eV, respectively. The results show that the band gap energy of the cubic structure perovskite is smaller than that of the tetragonal structure. Theoretical work has revealed the electron configuration of $MAPbI_3$, in that the valence band maximum is composed of antibonding combinations of Pb s and I p orbitals, and therefore any change to the perovskite lattice that increases the amount of Pb–I overlap will destabilize the valence band, raising it in energy. The conduction band, derived from p-orbitals and having poorer orbital overlap, is expected to respond less strongly to distortions in lattice structure than the valence band that is derived from Pb s orbitals.[16] In other words, organic cations change the metal–halide–metal bond by octahedral tilting, confirming two factors: (1) an increase in Pb–I overlap will decrease the band gap, or (2) a reduction in metal–halide overlap will increase the band gap. Metal–halide orbital overlap is a σ^* interaction, and reduction of the M–X–M bond angle reduces the extent of overlap between metals, and results in an increase in band gap energy.[17] From the XRD results, FA@$MAPbI_3$ and EA@$MAPbI_3$ have a cubic structure, while NH_4@$MAPbI_3$ and $MAPbI_3$ have a tetragonal structure. The metal–halide–metal bond angle in the cubic structure is close to 180°, while the tetragonal structure suffers from distortion, causing the metal–halide–metal bond angle to go below the value of 180° (Fig. S3, ESI†). Our work is in line with previous reports. Organic cations tune the band gap energy of the perovskite by changing the metal–halide–metal bond *via* tilting of the octahedra. In addition, we found that the band gap energy of the same structure perovskite crystals is also altered. For example, the band gap energy of NH_4@$MAPbI_3$ is bigger than that of $MAPbI_3$ and the band gap energy of EA@$MAPbI_3$ is bigger than that of FA@$MAPbI_3$. From the X-ray diffraction data we could easily find that the cell lattices of NH_4@$MAPbI_3$ and EA@$MAPbI_3$ are smaller than those of $MAPbI_3$ and FA@$MAPbI_3$, respectively. We suspect that lattice contraction could widen the band gap of perovskite crystals. This speculation needs to be verified by further theoretical and experimental research. In general, organic cations in perovskite materials tune the band gap energy *via* octahedral tilting or lattice contraction. Fig. 4 shows the schematic representation of band gap energy variation of mixed perovskite crystals.

To explore the thermal properties of perovskites, thermogravimetric analysis (TGA) was conducted from room temperature to 500 °C under nitrogen flow. For uniform temperature distribution, the large crystals were ground into a fine powder prior to testing. All the perovskites start to undergo about 20% mass loss of hydroiodic acid followed by about 7% loss of the organics at ~230 °C, except for FA@$MAPbI_3$ perovskite. FA@$MAPbI_3$ starts decomposition at 270 °C. This decomposition sequence indicates that the organic group is bound into the perovskite matrix more tightly than the HI. The thermal stability is related to the probability of HI formation, which is directly related to the acidity of the organic cation.[18] The stronger the acidic character of the cation, the higher the chance that the organic cation can be deprotonated to yield HI. Since the FA cation is less acidic than other organic species, it is natural that FA-incorporated perovskites possess the best thermal stability. Identical thermal behavior was also observed by differential scanning calorimetry (DSC), which is shown in Fig. 5(b). $MAPbI_3$ and NH_4@$MAPbI_3$

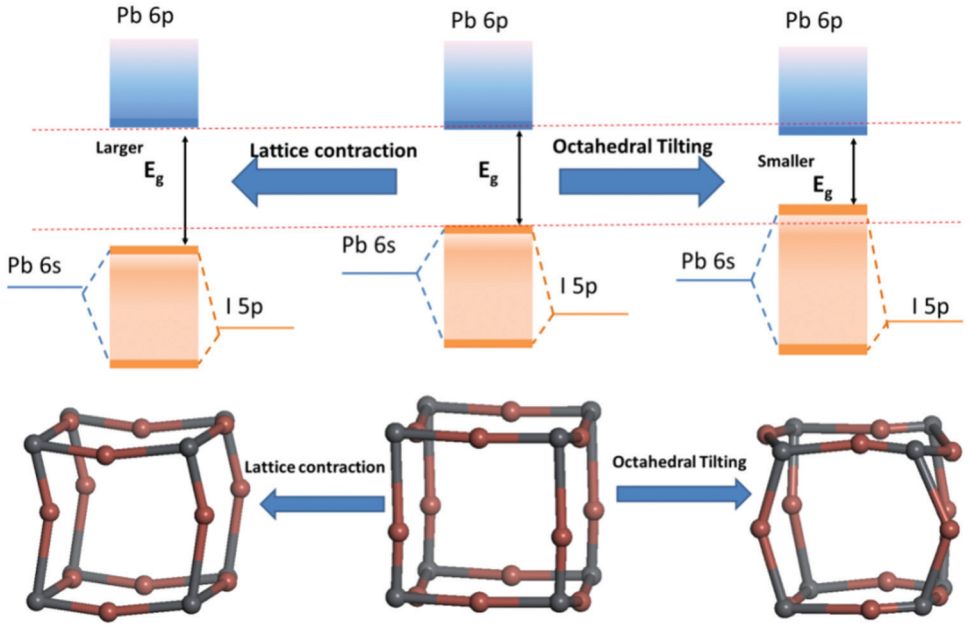

Fig. 4 Schematic representation of band gap energy variation of mixed perovskite crystals.

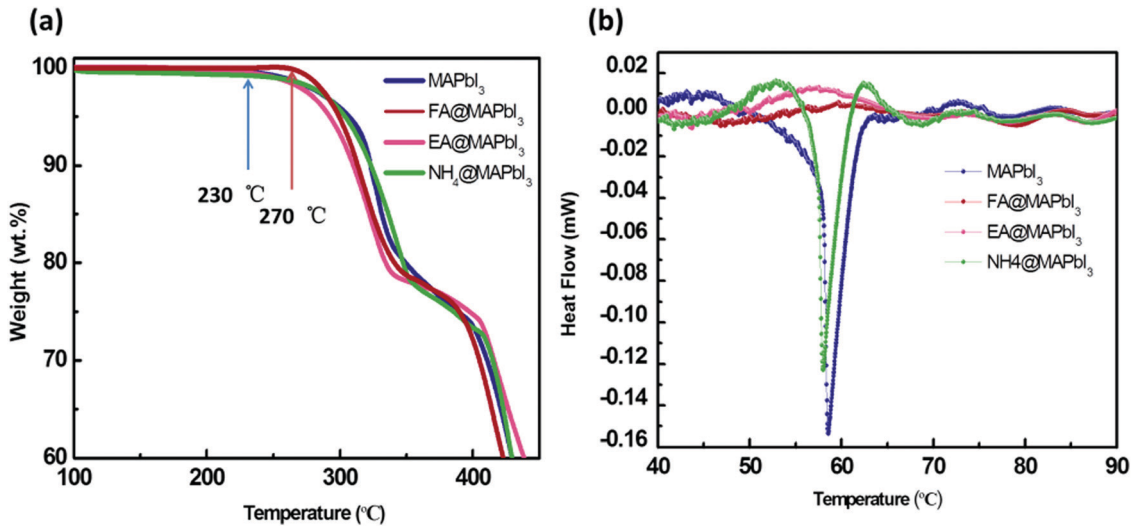

Fig. 5 (a) TGA curves of cubic phase crystals; (b) DSC heating curves of samples.

show a peak at 57 °C, which indicates a tetragonal–cubic phase transition. EA@$MAPbI_3$ and FA@$MAPbI_3$ perovskite crystals show a cubic phase at room temperature; hence no endothermic peak appears, indicating the improvement of thermodynamic stability.

To investigate the transport properties of perovskite single crystals, the trap density (n_{trap}) of the crystals was estimated. Voltage (V)–current (I) curves of Au/perovskite single crystal/Au hole-only devices were measured in the dark. When the applied voltage is lower than the kink-point voltage, the current I increases linearly with applied voltage V, demonstrating an ohmic response between the electrode and the perovskite for the hole-only device. As the applied voltage exceeds the kink-point voltage, the current I exhibits a quick non-linear increase, indicating that the trap states are fully filled by the injected carriers. The applied voltage at the kink point is defined as the trap-filled limit voltage (V_{TFL}), which is determined by the trap state density:[19]

$$V_{TFL} = \frac{en_{trap}L^2}{2\varepsilon\varepsilon_0} \quad (4)$$

where L is the thickness of the perovskite single crystal, ε is the relative dielectric constant, and ε_0 is the vacuum permittivity. Hence, the trap density, n_{trap}, can be calculated using eqn (1). Based on Fig. 6, the corresponding hole trap density values are 6.29×10^9 cm^{-3}, 7.36×10^9 cm^{-3}, 7.18×10^9 cm^{-3}, and 1.56×10^9 cm^{-3} for $MAPbI_3$, NH_4@$MAPbI_3$, EA@$MAPbI_3$, and FA@$MAPbI_3$, respectively. Compared with the previous report,[20] the trap density values of all four types of mixed perovskite crystals are

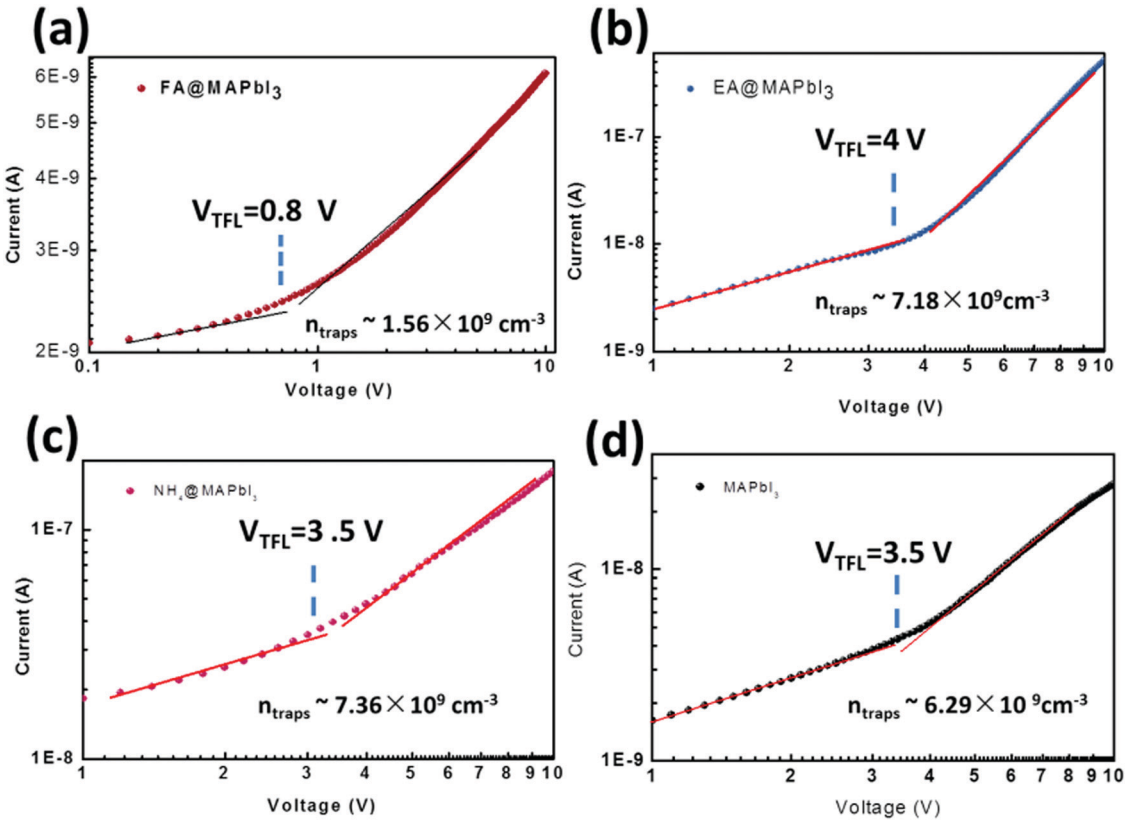

Fig. 6 Current–voltage curves for a hole-only perovskite device.

small, indicating the high quality of these crystals. The n_{trap} value in FA@MAPbI$_3$ is the lowest owing to its cubic phase and low lattice contraction degree.

Conclusions

In conclusion, four types of halide perovskite single crystals were grown to explore the effects of organic cations on various perovskite properties such as crystal structure, stability, and optoelectronic properties. Our findings suggest that: (1) the size of organic cations can not only cause lattice strain by lattice contraction or dilation but also may induce phase transitions by octahedral tilting; (2) precise band gap engineering is achieved by controlling bond angles; (3) thermal stability is related to the probability of HI formation, which is directly related to the acidity of the organic species; and (4) organic cations affect the transport property of crystals *via* affecting crystal structure. The cubic phase crystals have the lowest lattice strain and low trap density. These results represent an important step to highlight the role of organic cations in hybrid perovskite materials, which will further benefit the fundamental understanding of materials and device optimization.

Conflicts of interest

There are no conflicts to declare.

Acknowledgements

This work was supported by the National Natural Science Foundation of China (No. 61704153, 51572241, 61774019, and 51572033), Zhejiang Public Service Technology Research Program/Analytical Test (LGC19F040001), Visiting Scholar Foundation of State Key Lab of Silicon Materials (SKL2019-08), Fundamental Research Funds of Zhejiang Sci-Tech University (2019Q061, and 2019Q067) and the Natural Science Foundation of Zhejiang Province (No. LY20F040005)

References

1 Y. S. Chen, J. S. Manser and P. V. Kamat, All Solution-Processed Lead Halide Perovskite-BiVO$_4$ Tandem Assembly for Photolytic Solar Fuels Production, *J. Am. Chem. Soc.*, 2015, **137**(2), 974–981.

2 J. J. Choi, X. Yang, Z. M. Norman, S. J. L. Billinge and J. S. Owen, Structure of Methylammonium Lead Iodide Within Mesoporous Titanium Dioxide: Active Material in High-Performance Perovskite Solar Cells, *Nano Lett.*, 2014, **14**(1), 127–133.

3 G. Xing, N. Mathews, S. Sun, S. S. Lim, Y. M. Lam, M. Grätzel, S. Mhaisalkar and T. C. Sum, Long-range balanced electron- and hole-transport lengths in organic-inorganic $CH_3NH_3PbI_3$, *Science*, 2013, **342**(6156), 344.

4 K. A. Bush, A. F. Palmstrom, Z. J. Yu, M. Boccard, R. Cheacharoen, J. P. Mailoa, D. P. Mcmeekin, R. L. Z. Hoye, C. D. Bailie and T. Leijtens, 23.6%-efficient monolithic perovskite/silicon tandem solar cells with improved stability, *Nat. Energy*, 2017, **2**(4), 17009.

5 F. Xu, T. Zhang, G. Li and Y. Zhao, Mixed cation hybrid lead halide perovskites with enhanced performance and stability, *J. Mater. Chem. A*, 2017, **5**(23), 11450–11461.

6 N. J. Jeon, J. H. Noh, W. S. Yang, Y. C. Kim, S. Ryu, J. Seo and S. I. Seok, Compositional engineering of perovskite materials for high-performance solar cells, *Nature*, 2015, **517**(7535), 476.

7 Z. Li, M. Yang, J. Park, S. Wei, J. J. Berry and K. Zhu, Stabilizing Perovskite Structures by Tuning Tolerance Factor: Formation of Formamidinium and Cesium Lead Iodide Solid-State Alloys, *Chem. Mater.*, 2016, **28**(1), 284–292.

8 Y. Liu, Z. Yang, D. Cui, X. Ren, J. Sun, X. Liu, J. Zhang, Q. Wei, H. Fan and F. Yu, Two-Inch-Sized Perovskite $CH_3NH_3PbX_3$ (X = Cl, Br, I) Crystals: Growth and Characterization, *Adv. Mater.*, 2015, **27**(35), 5176–5183.

9 Y. Liu, Z. Yang, D. Cui, X. Ren, J. Sun, X. Liu, J. Zhang, Q. Wei, H. Fan and F. Yu, Two-Inch-Sized Perovskite $CH_3NH_3PbX_3$ (X = Cl, Br, I) Crystals: Growth and Characterization, *Adv. Mater.*, 2015, **27**(35), 5176.

10 M. Luan, J. Song, X. Wei, F. Chen and J. Liu, Controllable growth of bulk cubic-phase $CH_3NH_3PbI_3$ single crystal with exciting room-temperature stability, *CrystEngComm*, 2016, **18**(28), 5257–5261.

11 A. Amat, E. Mosconi, E. Ronca, C. Quarti, P. Umari, M. K. Nazeeruddin, M. Grätzel and A. F. De, Cation-induced band-gap tuning in organohalide perovskites: interplay of spin-orbit coupling and octahedra tilting, *Nano Lett.*, 2014, **14**(6), 3608.

12 H. S. Kim, H. I. Sang and N. G. Park, Organolead Halide Perovskite: New Horizons in Solar Cell Research, *J. Phys. Chem. C*, 2014, **118**(11), 5615–5625.

13 J. Torrent and V. Barrón, Diffuse Reflectance Spectroscopy of Iron Oxides, *Encycl. Surf. Colloid Sci.*, 2002, 1438–1446.

14 N. Ramanujam and G. M. Palmer, *Method for extraction of optical properties from diffuse reflectance spectra*, US, 2009.

15 A. E. Morales, E. S. Mora and U. Pal, Use of diffuse reflectance spectroscopy for optical characterization of unsupported nanostructures, *Rev. Mex. Fis.*, 2007, **53**(78), 18–22.

16 Y. H. Chang, C. H. Park and K. Matsuishi, First-principles study of the structural and the electronic properties of the lead-halide-based inorganic-organic perovskites $(CH_3NH_3)PbX_3$ and $CsPbX_3$ (X = Cl, Br, I), *J. Korean Phys. Soc.*, 2004, **44**(4), 889–893.

17 C. Grote and R. F. Berger, Strain Tuning of Tin–Halide and Lead–Halide Perovskites: A First-Principles Atomic and Electronic Structure Study, *J. Phys. Chem. C*, 2015, **119**(40), 150918142400006.

18 J. Yang, B. D. Siempelkamp, E. Mosconi, F. D. Angelis and T. L. Kelly, Origin of the Thermal Instability in $CH_3NH_3PbI_3$ Thin Films Deposited on ZnO, *Chem. Mater.*, 2015, **27**(12), 150529083734008.

19 Q. Dong, Y. Fang, Y. Shao, P. Mulligan, J. Qiu, L. Cao and J. Huang, Solar cells. Electron-hole diffusion lengths >175 μm in solution-grown $CH_3NH_3PbI_3$ single crystals, *Science*, 2015, **347**(6225), 967.

20 D. Shi, V. Adinolfi, R. Comin, M. Yuan, E. Alarousu, A. Buin, Y. Chen, S. Hoogland, A. Rothenberger and K. Katsiev, Solar cells. Low trap-state density and long carrier diffusion in organolead trihalide perovskite single crystals, *Science*, 2015, **347**(6221), 519.